Trioctylphosphine: A General Phosphorus Source for the Low-Temperature Conversion of Metals into Metal Phosphides

Amanda E. Henkes and Raymond E. Schaak*

Department of Chemistry, Texas A&M University, College Station, Texas 77842-3012

Received April 13, 2007. Revised Manuscript Received May 31, 2007

Metal phosphides can have important properties such as superconductivity, magnetoresistance, magnetocaloric behavior, catalytic activity, and lithium intercalation capacity, which make them useful for a variety of technological applications. Bulk metal phosphides usually require high temperatures and harsh reaction conditions to form, and metal phosphide nanocrystals can also be challenging to synthesize. Here we elaborate on a recently developed alternative approach for synthesizing metal phosphides, which involves the solution-mediated reaction of pre-formed metals with trioctylphosphine (TOP) at temperatures below 370 °C. This chemical conversion strategy is shown to be general and highly versatile, successfully forming a wide range of transition-metal and post-transition-metal phosphides using a range of both bulk and nanoscale metals as precursors. Metal nanocrystals, bulk powders, foils, wires, thin films, lithographically patterned substrates, and supported nanocrystals can all be converted to metal phosphides by reaction with TOP. Collectively, this represents a general, unified, and robust strategy for forming metal phosphides using readily available reagents and metal precursors.

Introduction

Transition-metal phosphides are important materials with a wide variety of useful physical properties, including superconductivity,[1] magnetocaloric behavior,[2] catalytic activity,[3−4] magnetoresistance,[5] and Li intercalation capacity for battery applications.[6−8] Bulk-scale metal phosphides are typically synthesized by direct combination of the elements at high temperatures, although reactive byproducts are often formed and must be separated from the desired phosphide product.[9] Metal fluxes can also be used to grow high-quality crystals of metal phosphides at lower temperatures than are necessary using direct reactions.[10] In recent years, methods have been developed for the synthesis of metal phosphide nanocrystals. In addition to providing access to high surface area catalysts and nanostructures with interesting morphology-dependent physical properties, these strategies offer a low-temperature solution-based alternative for forming crystalline metal phosphides. For example, solvothermal reactions,[11−12] thermal decomposition of single-source organometallic precursors,[13−14] and co-reaction of organometallic reagents with phosphines[15−19] have all been used to generate nanocrystalline phosphides. Most of these strategies focus on reactions of trioctylphosphine (TOP) with organometallic complexes of the 3d late transition metals. In some cases, high-quality shape-controlled metal phosphide nanocrystals with interesting physical properties can be generated.

Recently, several studies of metal phosphide formation using TOP as a phosphorus source have targeted the reactivity of metals (both in bulk form and as nanocrystals) with TOP, suggesting that metals can cause cleavage of the P−C bond, resulting in diffusion of phosphorus into the metal. For example, Khanna and co-workers explored the reactivity of bulk-scale In powder with TOP to form nanocrystalline InP.[19] Chen and co-workers hypothesized a

* To whom correspondence should be addressed. Phone: (979) 458-2858. Fax: (979) 845-4719. E-mail: schaak@mail.chem.tamu.edu.

(1) (a) Raub, C. J.; Zachariasen, W. H.; Geballe, T. H.; Matthias, B. T. *J. Phys. Chem. Solids* **1963**, *24*, 1093−1100. (b) DeLong, L. E.; Meisner, G. P. *Solid State Commun.* **1985**, *53*, 119−123.
(2) Tegus, O.; Brück, E.; Buschow, K. H. J.; de Boer, F. R. *Nature* **2002**, *415*, 150−152.
(3) Brock, S. L.; Perera, S. C.; Stamm, K. L. *Chem. Eur. J.* **2004**, *10*, 3364−3371.
(4) Oyama, S. T. *J. Catal.* **2003**, *216*, 343−352.
(5) Jiang, J.; Kauzlarich, S. M. *Chem. Mater.* **2006**, *18*, 435−441.
(6) Souza, D. C. S.; Pralong, V.; Jacobson, A. J.; Nazar, L. F. *Science* **2002**, *296*, 2012−2015.
(7) Bichat, M.-P.; Pascal, J.-L.; Gillot, F.; Favier, F. *Chem. Mater.* **2005**, *17*, 6761−6771.
(8) Mauvernay, B.; Doublet, M.-L.; Monconduit, L. *J. Phys. Chem. Solids* **2006**, *67*, 1252−1257.
(9) (a) Rundqvist, S. *Acta Chem. Scand.* **1961**, *15*, 451−453. (b) Zachariasen, W. H. *Acta Crystallogr.* **1963**, *16*, 1253−1255. (c) Gullman, L.-O. *J. Less-Common Met.* **1966**, *11*, 157−167.
(10) Kanatzidis, M. G.; Pöttgen, R.; Jeitschko, W. *Angew. Chem., Int. Ed.* **2005**, *44*, 6996−7023.
(11) (a) Su, H. L.; Xie, Y.; Li, B.; Liu, X. M.; Qian, Y. T. *Solid State Ionics* **1999**, *122*, 157−160. (b) Xie, Y.; Su, H. L.; Qian, X. F.; Liu, X. M.; Qian, Y. T. *J. Solid State Chem.* **2000**, *149*, 88−91. (c) Gu, Y.; Guo, F.; Qian, Y.; Zheng, H.; Yang, Z. *Mater. Res. Bull.* **2002**, *37*, 1101−1105.
(12) Aitken, J. A.; Ganzha-Hazen, B.; Brock, S. L. *J. Solid State Chem.* **2005**, *178*, 970−975.
(13) Lukehart, C. M.; Milne, S. B. *Chem. Mater.* **1998**, *10*, 903−908.
(14) Kim, Y.-H.; Jun, Y.-W.; Jun, B.-H.; Lee, S.-M.; Cheon, J. *J. Am. Chem. Soc.* **2002**, *124*, 13656−13657.
(15) (a) Perera, S. C.; Fodor, P. S.; Tosi, G. M.; Wenger, L. E.; Brock, S. L. *Chem. Mater.* **2003**, *15*, 4034−4038. (b) Perera, S. C.; Tsoi, G.; Wenger, L. E.; Brock, S. L. *J. Am. Chem. Soc.* **2003**, *125*, 13960−13961. (c) Gregg, K. A.; Perera, S. C.; Lawes, G.; Shinozaki, S.; Brock, S. L. *Chem. Mater.* **2006**, *18*, 879−886.
(16) Park, J.; Koo, B.; Yoon, K. Y.; Hwang, Y.; Kang, M.; Park, J.-G.; Hyeon, T. J. *Am. Chem. Soc.* **2005**, *127*, 8433−8440.
(17) Qian, C.; Kim, J.; Ma, L.; Tsui, F.; Yang, P.; Liu, J. *J. Am. Chem. Soc.* **2004**, *126*, 1195−1198.
(18) Chen, J.-H.; Tai, M.-F.; Chi, K.-M. *J. Mater. Chem.* **2004**, *14*, 296−298.
(19) Khanna, P. K.; Jun, K.-W.; Hong, K. B.; Baeg, J.-O.; Mehrotra, G. K. *Mater. Chem. Phys.* **2005**, *92*, 54−58.

10.1021/cm071021w CCC: $37.00
Published on Web 07/21/2007

catalytic cleavage of the P−C bond caused by reaction of TOP with nanocrystalline Fe (formed in situ) during formation of FeP.[18] Chiang and Chiang reacted Ni nanocrystals with TOP to form hollow Ni_2P nanospheres.[20] In all cases, experiments have shown that TOP is not merely an innocent coordinating ligand but rather a highly reactive compound that can serve as a stabilizer, solvent, and phosphorus source in the synthesis of metal phosphide nanocrystals.

Building on these prior studies, we recently reported a potentially general approach for synthesizing high-quality nanocrystals of transition-metal phosphides that was successful for a variety of 3d, 4d, and 5d transition-metal systems.[21] This method involves reacting pre-formed metal nanocrystals with TOP at 290−370 °C.[21] During this reaction phosphorus is liberated from TOP and diffuses into the metal nanoparticles, converting them to metal phosphides. This strategy was shown to be successful for generating nanocrystals of Ni_2P, PtP_2, Rh_2P, Au_2P_3, Pd_5P_2, and PdP_2.[21]

The reaction pathway that generates metal phosphide nanocrystals via "conversion chemistry" utilizes a diffusion-based mechanism. This approach differs from most previously reported methods for synthesizing high-quality metal phosphide nanocrystals with uniform sizes and well-defined shapes, which generally rely on formation and subsequent decomposition of organometallic complexes.[15−18] Our earlier results[21] imply that the shape, size, and size dispersity defined by the metal nanoparticle precursors can be retained in the metal phosphide product, providing a convenient route for generating high-quality nanocrystals of a large number of metal phosphide systems. Also, because metal phosphide nanocrystals are formed via diffusion of phosphorus into pre-formed metal nanoparticles, intricate hollow nanostructures are accessible because of Kirkendall effects,[20−22] which are not possible using thermal decomposition strategies. For example, we[21] and others[20] have exploited the Kirkendall mechanism to form hollow nanospheres of Ni_2P.

In this paper, we describe the results of our follow-up investigations aimed at exploring the versatility and establishing the generality of this "conversion chemistry" approach to the formation of metal phosphides. Specifically, we establish the range of 3d, 4d, and 5d transition-metal phosphide nanoparticles that are accessible by reacting the appropriate pre-formed metal nanoparticles with TOP. Furthermore, we show that, in some cases, even bulk-scale metal powders can be converted into metal phosphides by simple solution-mediated reactions with hot TOP. Using similar chemistry, metal wires, foils, films, and patterned microstructures can react with TOP to produce metal phosphide coatings and microscale metal phosphide features of variable thicknesses. In all cases, there is a remarkable correlation between the morphology of the metal precursors and the metal phosphide products. Taken together, these diverse synthetic capabilities demonstrate a very general, simple, and rapid solution-mediated strategy for accessing metal phosphides from pre-formed metals using convenient and commercially available reagents.

Experimental Section

All reactions were carried out under argon using standard air-free techniques.

Chemicals. All chemicals were used as purchased. Copper(II) 2,4-pentanedionate, iron(III) 2,4-pentanedionate, cobalt(II) 2,4-pentanedionate, and silver nitrate (99.9%) were purchased from Alfa Aesar. Tri-*n*-octylphosphine (tech. 90%), tri-*n*-octylphosphine oxide (TOPO), *n*-hexadecylamine (HDA, tech.), oleic acid (tech.), Ni powder (2.2−3.0 μm), Pd powder (0.25−0.55 and 0.5−1.7 μm), Zn powder (7 μm), Cu powder (−100 mesh), In powder (−325 mesh), Rh powder (−325 mesh), Ga pellets (6 mm diameter), Ni foil (0.01 mm thickness), and graphite (−325 mesh, conducting) were purchased from Alfa Aesar. Octyl ether (99%), oleylamine (70% tech.), 1,2-hexadecanediol (90% tech.), Zn wire (0.5 mm diameter), and Zn foil (0.5 mm diameter) were purchased from Sigma-Aldrich. Mossy Zn was from Matheson Coleman and Bell. Dodecenyl succinic anhydride, Araldite 502, and benzyldimethylamine were purchased from Electron Microscopy Sciences. LX 112 was purchased from Ladd Industries. S1827 positive photoresist and MF-319 developer were purchased from Shipley.

Characterization. Powder X-ray diffraction (XRD) was performed on a Bruker-AXS GADDS diffractometer as described previously.[23] Transmission electron microscopy (TEM) was performed using a JEOL JEM-2010 transmission electron microscope operating at 200 kV. TEM samples were prepared by sonicating a few milligrams of nanoparticles in either hexanes or ethanol (depending on solubility) and then drop casting onto Ni or Cu grids, which were allowed to slowly dry under ambient conditions (or in an argon atmosphere for more easily oxidized samples, such as Cu). Scanning electron microscopy (SEM) was performed using a JEOL JSM-6400 scanning electron microscope operating at 15 kV. Metal powders for SEM imaging were coated with AuPd using a sputter coater. Metal films and metal-patterned substrates were coated with conducting carbon using a metal evaporator to allow complete resolution of the phosphorus EDS signal. Optical spectroscopy was performed using a Perkin-Elmer Lambda 35 UV/vis spectrometer.

Cross sections of copper and copper phosphide wires were imaged using a Zeiss Axiophot confocal light microscope with color CCD camera. A copper wire and wires with copper phosphide coatings from various reaction times were embedded vertically in an epoxy resin. The epoxy resin was composed of 59.1% dodecenyl succinic anhydride (hardener), 15.9% LX 112 (epoxy resin component), 25% Araldite 502 (epoxy resin component), and 0.2 mL of benxyldimethylamine (accelerator). The resin was dried for 24 h at ∼50 °C. After drying, the cross-sectional surface of the wires was ground using a Buehler Ecomet grinder/polisher with 300, 600, and 1200 grit paper. The final stage of polishing was done with a polishing cloth and a 0.03 μm alumina powder slurry.

Metal Phosphide Nanocrystals. *Cu Nanocrystals.* This synthesis of copper nanocrystals is a modification of methods reported by Hyeon and co-workers for the synthesis of Ni nanocrystals.[24] A solution was prepared under Ar using 26.2 mg of $Cu(acac)_2$ in 1.000 mL of oleylamine, which was heated in a 100 °C water bath and then rapidly injected into 2.000 mL of oleylamine at 260 °C. The

(20) Chiang, R.-K.; Chiang, R.-T. *Inorg. Chem.* **2007**, *46*, 369−371.
(21) Henkes, A. E.; Vasquez, Y.; Schaak, R. E. *J. Am. Chem. Soc.* **2007**, *129*, 1896−1897.
(22) Yin, Y.; Rioux, R. M.; Erdonmez, C. K.; Hughes, S.; Somorjai, G. A.; Alivisatos, A. P. *Science* **2004**, *304*, 711−714.
(23) (a) Bhuvanesh, N. S. P.; Reibenspies, J. H. *J. Appl. Crystallogr.* **2003**, *36*, 1480−1481. (b) Bhuvanesh, N. S. P.; Reibenspies, J. H.; Zhang, Y.; Lee, P. L. *J. Appl. Crystallogr.* **2005**, *38*, 632−638.
(24) Park, J.; Kang, E.; Son, S. U.; Park, H. M.; Lee, M. K.; Kim, J.; Kim, K. W.; Noh, H.-J.; Park, J.-H.; Bae, C. J.; Park, J.-G.; Hyeon, T. *Adv. Mater.* **2005**, *17*, 429−434.

reaction was heated at 260 °C for 30 min and then slowly cooled. Cu particles could be isolated by saturating the solution with ethanol, followed by centrifugation and washing with ethanol and hexanes. For conversion to Cu_3P, the Cu was used as prepared in oleylamine to avoid oxidation.

Cu_3P Nanocrystals. A portion of the Cu nanocrystal solution in oleylamine (1.0 mL), prepared as described above, was mixed with 1.0 mL of TOP under Ar and then rapidly injected into 2.0 g of TOPO at 320 °C. The reaction was heated at 320 °C for 1 h and then slowly cooled and saturated with ethanol. Cu_3P nanocrystals were isolated by centrifugation, washed with ethanol, and dried under Ar.

Fe Nanocrystals. Synthesis of Fe nanocrystals is also a modification of a previous literature report.[24] A solution was prepared under Ar using 35.3 mg of $Fe(acac)_3$ in 1.0 mL of oleylamine, which was heated in a 100 °C water bath and then rapidly injected into 1.0 mL of oleylamine at 260 °C. The reaction was heated 1 h at 260 °C and then cooled to room temperature. This solution could be saturated with ethanol and centrifuged to isolate nanoparticles, although oxidation readily occurs.

FeP Nanocrystals. TOP (1.0 mL) was added to the Fe−oleylamine solution prepared as described above under Ar. This solution was stirred and then transferred via syringe pump into 2.0 g of HDA at 320 °C. The reaction was heated at 350 °C for 2 h and then slowly cooled and saturated with ethanol and hexanes. FeP particles were isolated by centrifugation, washed thoroughly with ethanol and hexanes, and dried under Ar.

Co Nanocrystals and in Situ Conversion to CoP. Synthesis of cobalt nanocrystals is also a modification of Hyeon's methods.[24] A solution was prepared under Ar using 30.9 mg of $Co(acac)_2$ in 1.0 mL of olyelamine, which was heated in a 100 °C water bath and then rapidly injected into 2.0 g of HDA at 320 °C. The reaction was heated 1 h at 320 °C; then the temperature was raised to 330 °C. At 330 °C, 1.0 mL of TOP was rapidly injected and the temperature was then raised to 370 °C. The reaction was held at 370 °C for 1 h and then slowly cooled and saturated with ethanol and hexanes. CoP particles were isolated by centrifugation, washed thoroughly with ethanol and hexanes, and dried under Ar. The Co nanocrystal intermediate could be isolated by saturating the solution with ethanol and hexanes prior to injection of TOP and centrifuging, although oxidation readily occurs.

Ag Nanocrystals. This synthesis is a modification of methods previously used by Sra et al. to prepare FePt nanocrystals.[25] A solution of 70.2 g of $AgNO_3$, 70.9 mg of 1,2-hexadecanediol, 100 μL of oleylamine, 100 μL of oleic acid, and 2.00 mL of octyl ether was heated at 100 °C for 1 h and then slowly cooled and saturated with ethanol, which caused an orange-brown precipitate to form. The precipitate was washed with hexanes several times. The hexane wash was reserved, to which an equal volume of ethanol was added. Ag nanocrystals were isolated by centrifugation from the hexane/ethanol solution, washed with ethanol, and dried under Ar.

AgP_2 Nanocrystals. TOP (1.0 mL) was added to 9.5 mg of Ag nanocrystals, and mixed by sonication, and then rapidly injected into 2.0 mL of TOP at 370 °C. The reaction was heated at 370 °C for 2 h and then slowly cooled and saturated with ethanol. A mixture of Ag and AgP_2 nanocrystals was isolated by centrifugation, washed with ethanol, and dried under Ar.

Bulk Metal Phosphide Powders. *Ni_2P Powder.* An aqueous solution of $NaBH_4$ (∼0.05 M) was prepared, and 2 mL was used to treat 12.2 mg of Ni powder (2.2−3.0 μm) to help minimize surface oxidation. The Ni powder was sonicated in the $NaBH_4$ solution, centrifuged and washed with copious amounts of water to remove $NaBH_4$ residue, and then dried under Ar. The treated Ni powder was heated at 300 °C in 2.0 mL of TOP for 2 h and then slowly cooled and saturated with ethanol. Ni_2P powder with a slight Ni impurity was isolated by centrifugation, washed thoroughly with ethanol, and dried under Ar.

Ni_5P_4 Powder. Ni_5P_4 powder was prepared identically to Ni_2P powder, except it was refluxed in TOP (370 °C) for 2 h. $NaBH_4$-treated Ni powder (15.4 mg, 2.2−3.0 μm) was used.

Zn_3P_2 Powder. Zn_3P_2 powder was prepared by refluxing 7.3 mg of Zn powder (7 μm) in 2.0 mL of TOP for 2 h, which was then slowly cooled and saturated with ethanol. Zn_3P_2 powder was isolated by centrifugation, washed thoroughly with ethanol, and dried under Ar.

Cu_3P/CuP_2 Powder. Cu powder (−100 mesh) was treated with dilute aqueous HCl (∼1.5 M) to remove surface oxidation and then thoroughly rinsed with Nanopure water and dried under Ar. The HCl-treated Cu powder (88.0 mg) was heated in 2.0 g of TOPO to 360 °C. At 360 °C, 2.0 mL of TOP was rapidly injected. The reaction was heated at 370 °C for 2 h and then slowly cooled and saturated with ethanol. A mixture of CuP_2 and Cu_3P powder was isolated by centrifugation, washed thoroughly with ethanol, and dried under Ar.

InP Powder. InP was prepared by first heating 111.0 mg of In powder (−325 mesh) in 2.0 mL of octyl ether to 290 °C. At 290 °C, 2.0 mL of TOP was rapidly injected. The reaction was heated at 325 °C for 2 h and then slowly cooled and saturated with ethanol. InP powder with an In metal impurity was isolated by centrifugation, washed thoroughly with ethanol, and dried under Ar.

Rh_2P Powder. Rh_2P was prepared by refluxing 15.6 mg of Rh powder (−325 mesh) in 3.0 mL of TOP for 1.5 h. At 1.5 h, 3.0 mL of TOP was injected. The reaction was heated a total of 6 h and then slowly cooled and saturated with ethanol. Rh_2P powder with a Rh metal impurity was isolated by centrifugation, washed thoroughly with ethanol, and dried under Ar

GaP Powder. GaP was prepared by refluxing an 18.6 mg Ga pellet in 2.0 mL of TOP for 2 h, which was then slowly cooled and saturated with ethanol. GaP powder with a Ga metal impurity was isolated by centrifugation, washed thoroughly with ethanol, and dried under Ar.

Pd_5P_2/PdP_2 Powders (size study). Investigations of the effect of metal precursor powder size on the phases formed were carried out using two sizes of Pd powder (0.25−0.55 and 0.5−1.7 μm) for reactions at 300 and 360 °C. The reactions at 300 °C were carried out using 15.0 mg of Pd powder (each size) and heating it in 2.0 mL of TOP at 300 °C for 2 h. The 360 °C reactions were carried out by heating 15.0 mg of Pd powder in 2.0 g of TOPO to 360 °C. At 360 °C, 2.0 mL of TOP was rapidly injected, and the reaction was further heated at 360 °C for 2 h. After heating, the reactions were slowly cooled and saturated with ethanol. Mixtures of Pd_5P_2 and PdP_2 powders were isolated by centrifugation, thoroughly washed with ethanol, and dried under Ar.

Metal Phosphide Foils and Wires. *Ni_2P Foil.* A piece of Ni foil (7.2 mg, 0.1 × 4 × 7 mm) was heated at 450 °C for 1.5 h in 5% H_2/95% Ar. It was then heated in 2.0 mL of TOP at 300 °C for 2 h and then slowly cooled and saturated with ethanol. The foil piece (now black) was washed thoroughly with ethanol and dried under Ar.

Zn_2P_3 Foil. A piece of Zn foil (0.24 g, 0.5 × 5 × 10 mm) was refluxed in 2.0 mL of TOP for 2 h and then slowly cooled and saturated with ethanol. The foil piece (now coated with black Zn_3P_2) was washed thoroughly with ethanol and dried under Ar.

Zn_3P_2 Wire, Mossy Lump. Zn wire (23.9 mg, 0.5 mm diameter, 1 cm length) was refluxed in 2.0 mL of TOP for 2 h and then

(25) Sra, A. K.; Ewers, T. D.; Xu, Q.; Zandbergen, H.; Schaak, R. E. *Chem. Commun*. **2006**, 750−752.

slowly cooled and saturated with ethanol. The wire had a black Zn_3P_2 coating after reaction and was washed thoroughly with ethanol and dried under Ar. Similarly, 0.1784 g of mossy Zn was refluxed in 2.0 mL of TOP for 3 h and then slowly cooled and saturated with ethanol. Likewise, it had a black Zn_3P_2 coating after reaction and was washed thoroughly with ethanol and dried under Ar.

CuP_2/Cu_3P Wires (time study). Cu wires (75 mg, 1 mm diameter, 1 cm length) were washed with dilute aqueous HCl (∼1.5 M) to remove any surface oxidation and then thoroughly rinsed with Nanopure water and dried under Ar. The wire pieces were refluxed for 30 min and 1, 2, and 4 h (separately) in 1.0 mL of TOP and then slowly cooled and saturated with ethanol. The wires (with a black, crystalline phosphide coating) were washed thoroughly and carefully with ethanol and dried under Ar.

Cu_3P/Cu Foil. Cu foil (0.1209 g, 0.2 × 5 × 10 mm) was washed with dilute aqueous HCl (∼1.5 M) to remove surface oxidation and thoroughly rinsed with Nanopure water and dried under Ar. The foil piece was refluxed in 1.0 g of HDA for 30 min (320 °C), and then 1.0 mL of TOP was rapidly injected. The reaction was refluxed 2 h more (350 °C) and then slowly cooled and saturated with ethanol. The foil piece (with a gray-black powdery coating) was washed thoroughly with ethanol and dried under Ar.

Cu_3P/CuP_2 Foil. Cu foil (0.2676 g, 0.5 × 10 × 15 mm) was washed with dilute aqueous HCl (∼1.5 M) to remove surface oxidation and thoroughly rinsed with Nanopure water and dried under Ar. The foil piece was refluxed in 2.0 mL of TOP for 2 h and then slowly cooled and saturated with ethanol. The foil piece (with a black, highly crystalline coating) was washed thoroughly with ethanol and dried under Ar.

Metal Phosphide Thin Films. *Zn Thin Film.* Zn thin films were made by depositing Zn onto precleaned glass microscope slides using a BOC Edwards Auto 306 Metal Evaporation Chamber. Zn wire was used as a Zn source. Zn (100 nm) was deposited onto 10 nm Cr. The resulting films were highly metallic and optically reflective but were not crystalline enough to obtain powder diffraction patterns.

Zn_3P_2 Thin Film. A Zn film on glass (1 × 3 cm glass slide) was refluxed in 2.0 mL of TOP for 2 h and then slowly cooled and saturated with ethanol. The Zn_3P_2 film (golden color and optically transparent) was washed thoroughly with ethanol and dried under Ar.

Au Thin Film. A Au thin film was prepared by slowly evaporating an aqueous solution of $HAuCl_4 \cdot 3H_2O$ onto a precleaned glass microscope slide. The glass slide was placed vertically in a scintillation vial, which was filled with aqueous $HAuCl_4$ solution and allowed to slowly evaporate while covered with a crystallization dish for 5 weeks. The glass was then heated at 500 °C for 2 h in 5% H_2/95% Ar to reduce the Au^{3+} to Au^0.

Au/Au_2P_3 Thin Film. A 1.25 × 1.5 cm piece of Au-coated glass was refluxed in 2.0 mL of TOP for 6 h total (with 1.0 mL of TOP injected at 2 and 3 h) and then slowly cooled and saturated with ethanol. The Au/Au_2P_3 film was washed thoroughly with ethanol and dried under Ar.

Supported Metal Phosphide Nanocrystals. *Graphite-Supported Ni Nanocrystals.* This synthesis is a modification of that used by Hyeon et al. for making Ni nanocrystals.[24] Supported Ni nanocrystals were prepared by heating 0.1110 g of $Ni(acac)_2$, 0.7604 g of graphite (−325 mesh, conducting), and 1.0 mL of oleylamine in 6.0 g of triphenylphosphine at 220 °C for 30 min, which was then slowly cooled and saturated with ethanol. A black powder was isolated via centrifugation, washed thoroughly with ethanol, and dried under Ar.

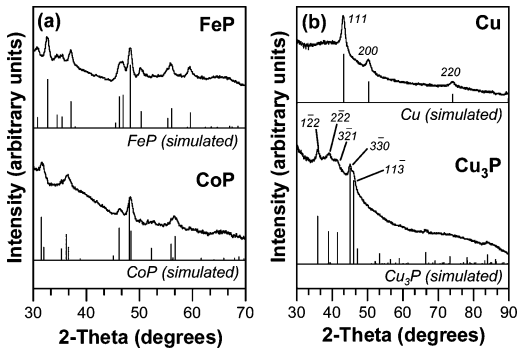

Figure 1. Powder XRD patterns of (a) FeP and CoP nanocrystals formed by reacting their respective metal nanoparticles with hot TOP and (b) Cu nanocrystals and Cu_3P made by reacting Cu nanocrystals with hot TOP. The broad feature between 30° and 40° 2θ is due to amorphous copper oxide, which forms by air oxidation of the copper nanocrystals.

Graphite-Supported Ni_2P Nanocrystals. Ni on graphite (29.0 mg) was heated in 2.0 mL of octyl ether to 290 °C. At 290 °C, 1.0 mL of TOP was rapidly injected. The reaction was heated at 300 °C for 2 h and then slowly cooled and saturated with ethanol. The powder was isolated via centrifugation, washed thoroughly with ethanol, and dried under Ar.

Metal Phosphide Patterned Substrates. *Cu Patterns on Glass.* Glass microscope slides were annealed at 450 °C for 4 h, washed thoroughly with isopropanol and acetone, and dried with a stream of air. S1827 positive photoresist was spin coated onto the microscope slides at 2000 rpm (∼3.5 μm thickness) using a SCS P6204 (8-in. bowl) nonprogrammable spin coater. The photoresist-coated glass slides were exposed to UV light using a Quintel Q4000 MA mask aligner and a mask with 0.2 mm × 10 mm stripes. The exposed slide was developed in MF-319 developer, rinsed with deionized water, and dried with a stream of air. The photopatterned glass was then coated with 100 nm of Cu using a BOC Edwards Auto 306 Metal Evaporation Chamber. Photoresist and excess Cu were lifted off by lightly sonicating the coated glass in deionized water, leaving behind Cu stripes on glass.

Cu_3P from Cu Patterns on Glass. Cu-patterned glass slides were cut to ∼1 × 2 cm pieces. The patterned glass was heated at 320 °C in 4 mL of TOP under Ar for 30 min and then slowly cooled and saturated with ethanol. The pattern on the glass turned a silvery-gray color after completion of the reaction. The liquid was decanted, and the patterned glass was rinsed several times with ethanol and then dried under Ar.

Results and Discussion

Converting Metal Nanoparticles to Nanocrystalline Metal Phosphides. Our initial work, predominantly with the Ni−P system, showed that Ni nanoparticles could be converted to Ni_2P nanoparticles upon reaction with TOP in octyl ether at 300 °C.[21] There is some evidence that Ni_5P_4 nanoparticles can be generated as well, but this has not been thoroughly studied. A similar reaction can also be used to generate nanocrystalline FeP and CoP (Figure 1a). For FeP, Fe nanoparticles are synthesized by thermal decomposition of an $Fe(acac)_3$−oleylamine complex in hot oleylamine; then a portion of the Fe−oleylamine solution is mixed with TOP, injected into refluxing HDA, and heated at 350 °C for 1−2 h to form FeP. The Fe nanoparticles cannot be isolated or characterized without oxidizing to Fe_2O_3, but their presence is inferred based on the synthetic protocol and the fact that the Fe_2O_3 nanoparticles that are isolated cannot be converted

to FeP by reaction with TOP. CoP nanocrystals can be synthesized using a similar protocol (Figure 1a). Nanocrystals of both FeP and CoP have been reported previously using other methods,[15a,17−18,26] so we will not focus on these systems.

Cu_3P nanocrystals can also be generated by reacting Cu nanoparticles with TOP in TOPO at 320 °C. Several literature reports describe the synthesis of nanocrystalline or bulk-scale Cu_3P using solvothermal strategies,[11a−b,12] but no examples of high-quality single-domain Cu_3P nanocrystals with minimal polydispersity have been reported previously. Figure 1b shows powder XRD data for Cu nanoparticles as well as Cu_3P formed from reaction of Cu nanoparticles with hot TOP. The Cu nanoparticles are generally spherical with an average size of 13.1 ± 2.6 nm (Figures 2a and S1). The SAED pattern confirms the fcc structure of Cu metal (Figure 2a). After reaction with TOP to form Cu_3P, the nanoparticles grow to 15.6 ± 2.6 nm (consistent with diffusion of P into Cu) while retaining the general morphology and size dispersity of the Cu nanoparticle precursors (Figures 2b and S1). The SAED pattern (Figure 2b) confirms that the nanoparticles are Cu_3P, and EDS analysis shows a Cu:P ratio of 55:45 (Figure 2b). This is consistent with the ratio expected from formation of Cu_3P stabilized by TOP, which increases the amount of phosphorus detected by EDS. The Cu_3P nanoparticles are generally single-domain crystals (Figure 2c), and their morphology tends to feature hexagonal facets that are derived from the hexagonal crystal structure of Cu_3P (Figure 2d).

Table 1 summarizes the key synthetic conditions and accessible phases of all of the late-transition-metal phosphides that are accessible as nanocrystalline solids by reacting metal nanoparticles with hot TOP. Our earlier work focused primarily on Ni_2P as well as 4d (Rh_2P, Pd_5P_2, PdP_2) and 5d (PtP_2, Au_2P_3) transition-metal phosphides.[21] Our new entries are FeP, CoP, Cu_3P, and AgP_2. It was found that Ir, Sn, and Ru nanoparticles did not form phosphides under the conditions used for the other systems, perhaps due to reactivity (Ir) or oxidation (Sn, Ru). AgP_2 (Figure S2) always has significant Ag impurities, indicating that the reaction does not go to completion. This is analogous to the Au−P system, which also shows a mixture of metal and metal phosphide. By TEM both the Au−P and Ag−P systems show particles that are significantly larger (∼500 nm) than the precursors (∼5−10 nm). Thus, the incomplete reactions may be a consequence of the significantly larger particle sizes, likely due to irreversible coalescence during synthesis.

It is worth highlighting that we (and others) generally observe that only one or two phases form preferentially in a particular binary system that contains multiple line phases. For metal phosphides the phases that form as nanocrystals tend to be those that are stable to the highest temperatures (regardless of whether they are metal-rich or phosphorus-rich), but this is not always the case. Thus, it is difficult to predict in which systems multiple phases will be accessible. In systems where multiple metal phosphide phases can be formed, higher temperatures tend to favor the phosphorus-rich phases because of either higher phosphorus availability via TOP decomposition or faster phosphorus diffusion into the metal nanoparticles. Exploiting other solution-chemistry conversion strategies could possibly expand the number of accessible phases in a given binary system.[27]

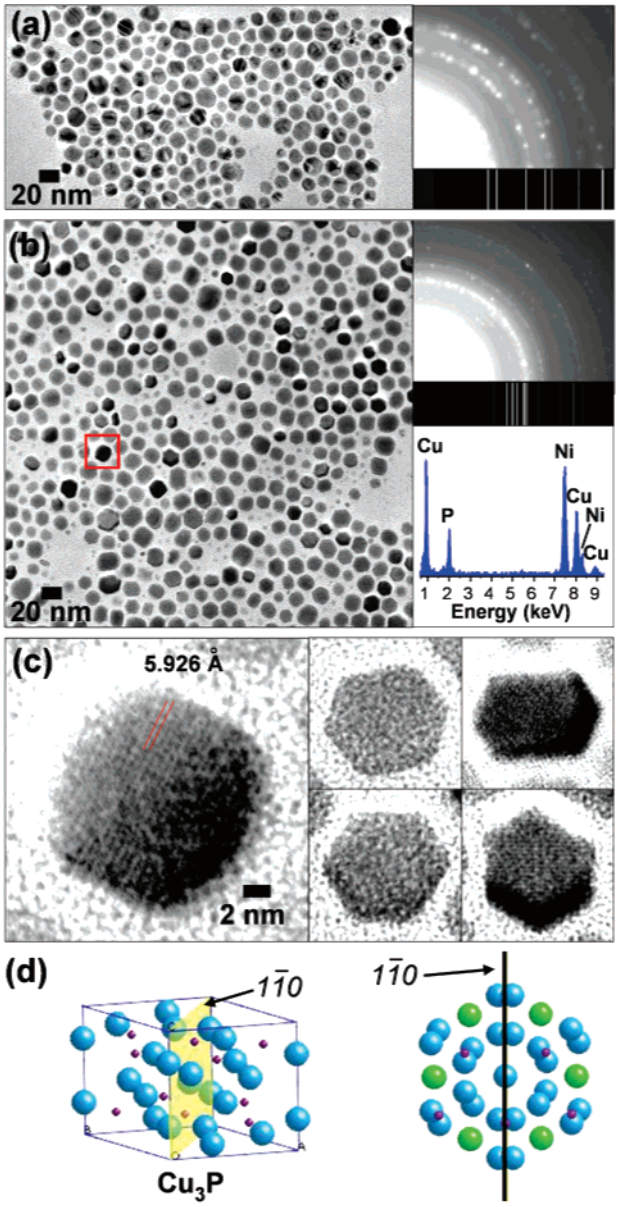

Figure 2. Cu_3P nanocrystals formed by reacting Cu nanoparticles with hot TOP: (a) TEM image, SAED pattern, and a simulated diffraction pattern for Cu nanoparticle precursors; (b) TEM image, SAED pattern, a simulated diffraction pattern, and EDS data (Ni grid) for Cu_3P nanocrystals formed from a; (c) TEM images of Cu_3P nanocrystals showing their predominant hexagonal morphology. An enlarged high-resolution image, highlighted in red in panel b, shows a *d* spacing corresponding to the 110 plane of Cu_3P; (d) unit cell of Cu_3P with 1$\bar{1}$0 plane highlighted, and top view of several unit cells (viewed down the 110 plane) showing how the Cu_3P crystal structure is related to the observed hexagonal morphology of the nanocrystals (corner Cu atoms of hexagon motif are highlighted green, other Cu atoms are blue; phosphorus atoms are red).

Converting Bulk Metal Powders to Metal Phosphides. Despite the limited reactivity observed for larger particle sizes

(26) Li, Y.; Malik, A.; O'Brien, P. *J. Am. Chem. Soc.* **2005**, *127*, 16020−16021.

(27) (a) Cable, R. E.; Schaak, R. E. *J. Am. Chem. Soc.* **2006**, *128*, 9588−9589. (b) Leonard, B.M.; Schaak, R.E. *J. Am. Chem. Soc.* **2006**, 11475−11482.

Table 1. Transition-Metal Phosphides Accessible by Reacting Metal Nanocrystal Precursors with TOP

nanocrystal precursor	reaction conditions[a]	product (via powder XRD)
Fe	350 °C HDA/TOP, 2 h	FeP
Co	350 °C HDA/TOP, 2 h	CoP
Ni	300 °C TOP/Oct_2O, 2 h	Ni_2P
Cu	320 °C TOP/TOPO, 1 h	Cu_3P
Rh	360 °C TOP/TOPO, 2 h	Rh_2P
Ag	370 °C TOP, 2 h	AgP_2, Ag
Pd	300 °C TOP, 0.5 h	Pd_5P_2
	360 °C TOP/TOPO, 2 h	PdP_2
Pt	370 °C TOP/TOPO, 2 h	PtP_2
Au	360 °C TOP/TOPO, 6 h	Au_2P_3, Au

[a] HDA = *n*-hexadecylamine, TOP = tri-*n*-octylphosphine, TOPO = tri-*n*-octylphosphine oxide, Oct_2O = octyl ether.

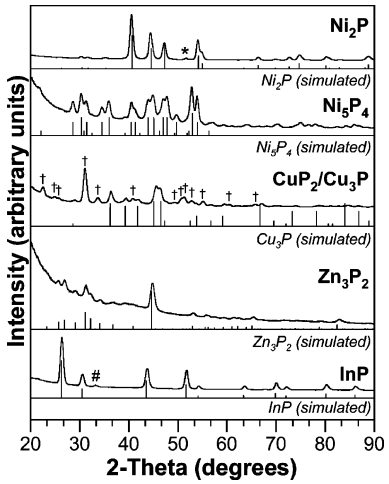

Figure 3. Powder XRD patterns for metal phosphides made from bulk metal powders. Ni metal and In metal impurities are represented by * and #, respectively. CuP_2 is represented by † in mixed-phase Cu_3P/CuP_2.

in the Ag−P and Au−P systems, size-dependent studies in several other systems have revealed that the reactivity of metals with hot TOP to form metal phosphides is apparently not always limited to nanocrystalline metals. Figure 3 shows representative powder XRD data for metal phosphide powders that form from the reaction of commercially available bulk-scale metal powders with TOP, typically under reflux conditions. (As-purchased microcrystalline powders of Mn, Fe, Nb, Ru, W, Ir, Al, Si, and Sn were found not to convert to metal phosphides under these conditions, although modifications to the procedure may facilitate similar conversions in the future.) For example, Ni_2P forms by heating 2.2−3.0 μm Ni powder in TOP at 300 °C, while the phase that forms upon heating the same Ni powder in TOP at 370 °C is Ni_5P_4 (Figure 3). Intermediate temperatures result in a mixture of Ni_2P and Ni_5P_4. As we observed previously for Pd−P nanocrystals[21] and now for Ni−P bulk powders, varying the reaction temperature can provide access to multiple phases in some metal−phosphorus systems.

When Cu powder is heated to reflux in TOP, a mixture of CuP_2 and Cu_3P is formed (Figure 3); a phase-pure copper phosphide has not been obtained, although no unreacted Cu remains (as determined by XRD). We hypothesize, based on observations of reactivity of TOP with Cu wires, that Cu_3P forms first on the surface of the Cu crystallites with CuP_2 growing in as more phosphorus is available for diffusion. The fact that pure Cu_3P can be obtained as nanocrystals is likely attributable to the size of the Cu source, which is quickly consumed by initial formation of Cu_3P. Consistent with this, there is some evidence that nanocrystalline CuP_2 can form upon further reaction of Cu_3P nanocrystals with TOP at reflux. Bulk Pd reacts similarly, always forming a mixture of PdP_2 and Pd_5P_2 (Figure S3). This is in contrast to the reactivity of Pd nanoparticles, which can be made to form pure PdP_2 (360 °C) and pure Pd_5P_2 (300 °C).[21] When Pd powder with an average particle size of 0.25−0.55 μm is used, the PdP_2:Pd_5P_2 ratio is approximately 40:60 at 300 °C. Likewise, 0.5−1.7 μm Pd forms PdP_2 and Pd_5P_2 in a ratio of approximately 25:75 at 300 °C. This indicates that larger particle sizes tend to favor formation of Pd_5P_2 relative to PdP_2, perhaps because of diffusion constraints in the larger Pd particles. Other bulk metal powders convert incompletely. For example, Rh powder forms a mixture of Rh_2P and Rh (Figure S4), possibly with Rh_2P passivating the Rh particles and preventing or hindering further reaction.

Zn powder can also be reacted with TOP to form Zn_3P_2, which is an important material for photovoltaic applications,[28] lithium-ion battery anodes,[2] and agricultural pesticides.[29] Figure 3 shows the formation of Zn_3P_2 without any residual Zn. (Zn_3P_2 nanocrystals have not been prepared using this strategy because isolatable Zn nanoparticle precursors could not be prepared by standard methods. Zn_3P_2 nanocrystals and films have been prepared by other methods however.[30−32]) InP can also form from reaction of In metal with TOP, although a small In impurity remains. This behavior is consistent with, and slightly improved upon, that observed previously for the incomplete reaction of In with TOP.[19] Table 2 summarizes all of the phases of metal phosphides that are accessible from bulk metal precursors as well as the key reaction conditions that generate each phase.

SEM micrographs of representative metal powder precursors and their resulting metal phosphide products show that the overall morphology (e.g., general aggregate size and shape) is retained, but the fine microstructure of the metal powders is lost upon reaction with hot TOP. For example, the commercially available 7 μm Zn powder that we used as a precursor consists of spherical aggregates of smaller (~800 nm), irregularly shaped Zn particles (Figure 4a). After conversion to Zn_3P_2, the average size of the aggregates remains similar. However, within the aggregates the primary particles are notably larger and fused together, although remnants of the original aggregate structure are still observable (Figure 4b). Similarly, the Ni powder precursor (Figure 4c) retains its overall spherical morphology and size after conversion to Ni_2P and Ni_5P_4 (Figure 4d,e), but reaction with TOP produces nickel phosphides that have lost the sharp

(28) (a) Hermann, A. M.; Madan, A.; Wanlass, M. W.; Badri, V.; Ahrenkiel, R.; Morrison, S.; Gonzales, C. *Sol. Energy Mater. Sol. Cells* **2004**, *82*, 241−252. (b) Soliman, M.; Kashyout, A. B.; Osman, M.; El-Gamal, M. *Ren. Energy* **2005**, *30*, 1819−1829.
(29) Hygnstrom, S. E.; McDonald, P. M.; Virchow, P. M. *Int. Biodet. Biodeg.* **1998**, *42*, 147−152.
(30) Buhro, W. E. *Polyhedron* **1994**, *13*, 1131−1148.
(31) (a) Pawlinkowski, J. M. *Phys. Rev. B* **1982**, *26*, 4711−4713. (b) Bryja, L.; Jezierski, K.; Misiewicz, J. *Thin Solid Films* **1993**, *229*, 11−13.
(32) (a) Green, M.; O'Brien, B. *Chem. Mater.* **2001**, *13*, 4500−4505. (b) Weber, A.; Sutter, P.; von Känel, H. *J. Appl. Phys.* **1994**, *75*, 7448−7455.

Table 2. Bulk-Scale Metal Phosphides Accessible Using a Variety of Metal Precursors

bulk metal precursor	reaction conditions[a]	product (via powder XRD)
Zn powder	370 °C TOP, 2 h	Zn_3P_2
wire	370 °C TOP, 2 h	Zn_3P_2
foil	370 °C TOP, 2 h	Zn_3P_2
mossy	370 °C TOP, 2 h	Zn_3P_2, Zn
film	370 °C TOP, 2 h	Zn_3P_2
Ni powder	300 °C TOP, 2 h	Ni_2P, Ni
	370 °C TOP, 2 h	Ni_5P_4
foil	300 °C TOP, 2 h	Ni_2P
	370 °C TOP, 2 h	Ni_2P, Ni_5P_4
Cu powder	370 °C TOP/TOPO, 2 h	Cu_3P, CuP_2
foil	350 °C HDA/TOP, 2 h	Cu_3P, Cu
	370 °C TOP, 2 h	Cu_3P, CuP_2
wire	370 °C TOP, 0.5-2 h	CuP_2, Cu_3P (time dependent)
patterned glass	320 °C TOP, 0.5 h	Cu_3P (characterized by EDS)
Rh powder	370 °C TOP, 6 h	Rh_2P, Rh
Ga pellet	370 °C TOP, 2 h	GaP, Ga
In powder	325 °C TOP/Oct_2O, 2 h	InP, In
Pd powder (0.25−0.55 μm)	360 °C TOP/TOPO, 2 h	PdP_2, Pd_5P_2 (~30% Pd_5P_2)
	300 °C TOP, 2 h	Pd_5P_2, PdP_2 (~60% Pd_5P_2)
Pd powder (0.5−1.7 μm)	360 °C TOP/TOPO, 2 h	PdP_2, Pd_5P_2 (~45% Pd_5P_2)
	300 °C TOP, 2 h	Pd_5P_2, PdP_2 (~75% Pd_5P_2)
Au film	370 °C TOP, 6 h	Au_2P_3, Au

[a] HDA = *n*-hexadecylamine, TOP = tri-*n*-octylphosphine, TOPO = tri-*n*-octylphosphine oxide, Oct_2O = octyl ether.

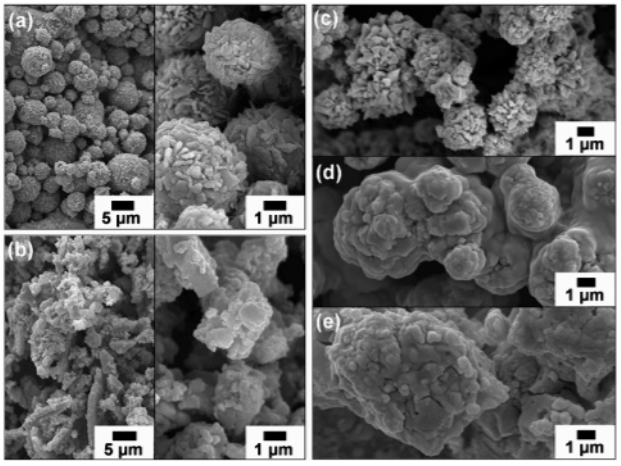

Figure 4. SEM images of metal precursor powders and the metal phosphide powders formed from them: (a) 7 μm Zn powder, (b) Zn_3P_2 formed from a, (c) 2.2−3.0 μm Ni powder, (d) Ni_2P, and (e) Ni_5P_4 formed from c.

facets of the Ni crystallites in the precursor powder. Overall, the conversion of micrometer-sized bulk powders to metal phosphides is a harsh reaction that changes the fine microstructure of the metal but manages to retain the average mesh size and morphology of the metal powder precursor. Analogous reactions with nanocrystals appear to proceed with less aggregation and change of nanostructure because surface stabilizers are present and the particles are more easily dispersible in the solvent (and thus remain better separated from one another).

Coating Metal Wires and Foils with Metal Phosphides. In addition to powders, other bulk-scale metals such as wires and foils also react with hot TOP to form metal phosphides. Unlike the micrometer-sized metal powders, which often convert completely to metal phosphides, the metal wires and foils react with TOP to form coatings with penetration depths typically approaching several hundreds of micrometers. For example, when mossy Zn is reacted under conditions that

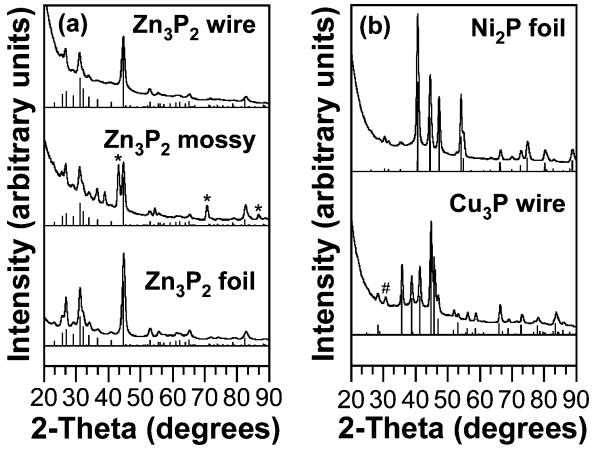

Figure 5. (a) Powder XRD patterns for Zn_3P_2 coatings made from various Zn precursors (Zn impurity is represented by *); (b) Ni_2P made from Ni foil and Cu_3P wire coating (with CuP_2 impurity represented by #) made from Cu wire.

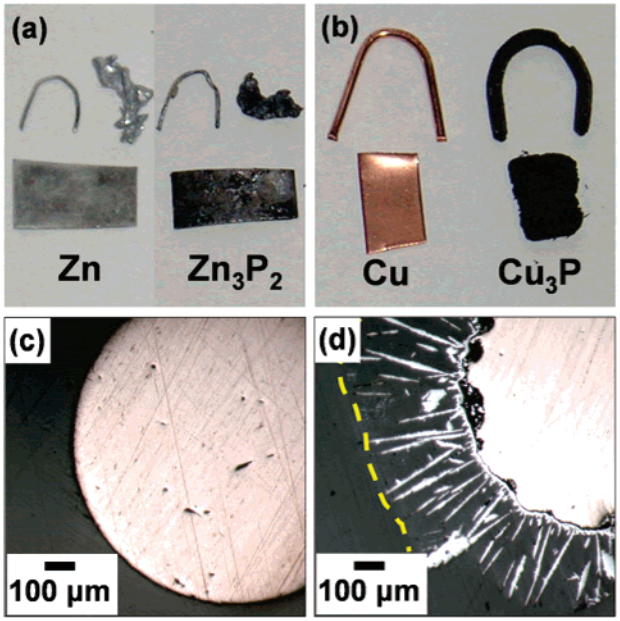

Figure 6. Digital photographs of (a) Zn wire, foil, and mossy pieces and Zn_3P_2 coatings made by refluxing these bulk solids in TOP, (b) Cu metal wire and foil and the wire and foil with a thick Cu_3P coating (with CuP_2 impurity) made by refluxing in TOP, (c) cross-sectional view of 1 mm diameter Cu wire, and (d) a resulting ~300 μm Cu_3P/CuP_2 coating formed around the Cu wire after refluxing in TOP for 30 min. The dotted yellow line indicates where the coating ends.

are analogous to those used for Zn powder, a coating of Zn_3P_2 is readily formed. Similar reactivity occurs for Zn wire and foil. Powder XRD data for Zn_3P_2-coated mossy Zn, Zn wire, and Zn foil are shown in Figure 5a, and digital photographs of the precursors and products are shown in Figure 6a. Similarly, Ni foil can be coated with Ni_2P (Figure 5b). Cu foil and wire can also be coated with Cu_3P/CuP_2 by refluxing in TOP (Figures 5b and 6b).

Insight into the penetration depth of the phosphide coatings is shown in Figure 6c,d. In this experiment a Cu wire (Figure 6c) and a Cu wire refluxed in TOP for 30 min (Figure 6d) were embedded vertically in an epoxy resin, and the polished cross-sectional surface was imaged using an optical microscope. The Cu wire cross section (1 mm diameter) shows no visible surface coating (Figure 6c). However, the Cu wire coated with predominantly Cu_3P (along with a small amount

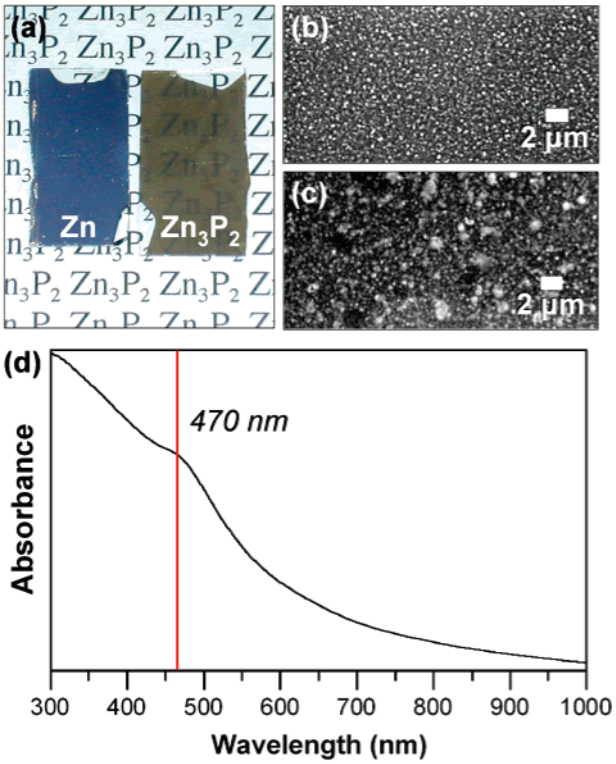

Figure 7. Zn_3P_2 film made by reacting thermally evaporated 100 nm Zn film with hot TOP: (a) digital photograph comparing Zn film precursor with transparent Zn_3P_2 product; SEM images of (b) Zn film and (c) Zn_3P_2 film; (d) optical spectrum of Zn_3P_2 film with λ_{max} at ~470 nm.

of CuP_2) reveals a Cu metal core (with a diameter that has decreased to 0.95 mm) surrounded by a ~300 μm phosphide coating.

Converting Metal Films, Supported Nanoparticles, and Patterned Substrates to Metal Phosphides. In addition to nanocrystalline and bulk metals, nanostructured and patterned metals can also be converted to metal phosphides with retention of the characteristic features of the nanoscale metal precursors. For example, thin films of Zn (100 nm) made by thermally evaporating Zn metal onto a clean glass slide (with 10 nm Cr adhesion layer between glass and Zn) can be refluxed in TOP to form Zn_3P_2 films (Figure 7a). SEM images shown in Figure 7b,c show how the surface of the film changes during reaction with TOP. The Zn film coarsens after refluxing in TOP for 2 h to form Zn_3P_2. EDS shows a Zn:P ratio of 42:58 for the Zn_3P_2 film (Figure S5). The Zn_3P_2 film is optically transparent with a peak at ~470 nm in the UV−vis spectrum (Figure 7d), corresponding to a blue shift relative to bulk Zn_3P_2.[31] This is consistent with quantum confinement effects previously reported for Zn_3P_2 films and nanocyrstals.[31b,32] Zn_3P_2, a semiconductor with a band gap in the range of visible light (1.51 eV),[31] has had recent interest as a low-cost semiconductor for use in hybrid solar cells because it absorbs light at the most intense wavelength of sunlight.[28,31−32] Reactions of Zn films, which are easily deposited by thermal evaporation, with TOP, a commercially available reagent, may provide a convenient alternative method for producing Zn_3P_2-based solar cells.

In addition to metal films, metal nanoparticles immobilized on high surface area supports for applications in catalysis can also be converted to supported metal phosphides by

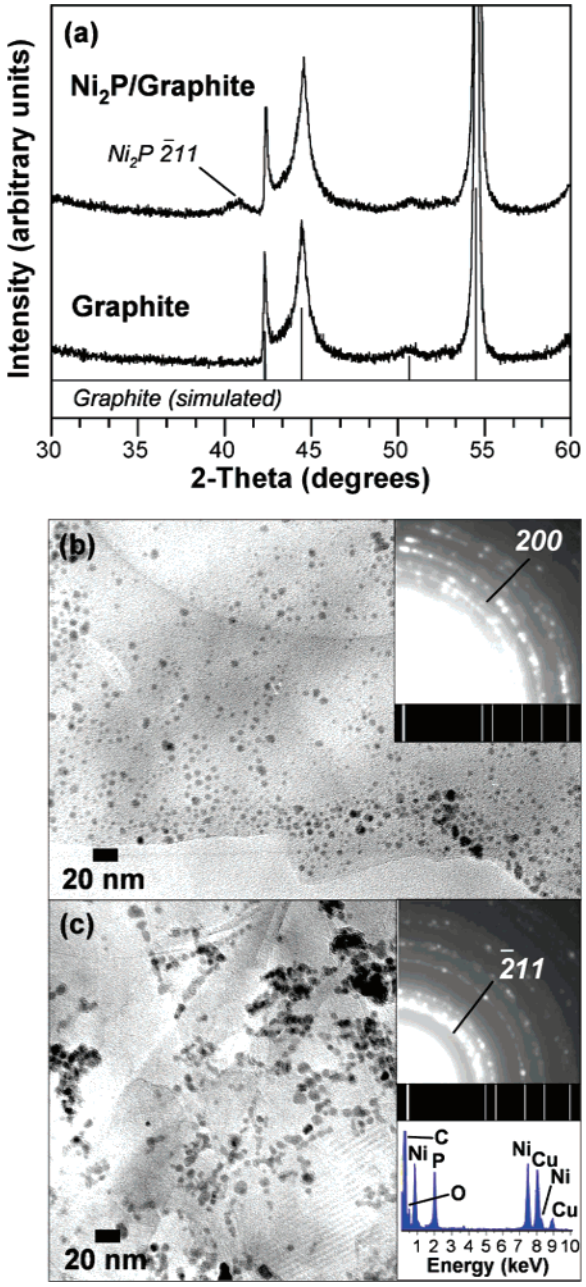

Figure 8. (a) Powder XRD pattern for graphite and Ni_2P nanoparticles supported on graphite. TEM images for (b) Ni on graphite and (c) Ni_2P formed from the reaction of b with TOP at 300 °C. Both SAED patterns show simulated graphite peaks as well as the key peaks attributable to Ni and Ni_2P in b and c, respectively. The EDS plot in c shows the presence of both Ni and P (a Cu TEM grid was used).

reaction with TOP. Ni_2P is known to be highly active for hydrodesulfurization reactions and is superior to traditional hydrotreating catalysts such as sulfided Ni−Mo, which becomes deactivated over time due to sulfur build-up that changes the surface chemistry of the catalyst.[4] Ni nanocrystals supported on graphite can be made by heating a solution of $Ni(acac)_2$ and graphite in oleylamine and triphenylphosphine at 220 °C for 30 min. The graphite-supported Ni nanoparticles can be isolated easily by centrifugation, washed with ethanol, dried under Ar, and re-dispersed in octyl ether. After injecting TOP into a 290 °C octyl ether suspension of the graphite-supported Ni nanoparticles and aging at 300 °C for 2 h, the supported Ni nanoparticles convert to Ni_2P while remaining on the support. Characterizing graphite-supported

Ni nanoparticles by XRD is challenging because of the significant peak broadening and the presence of peaks that overlap with those of graphite. The peak broadening is consistent with XRD data reported for nonsupported Ni nanoparticles made by a similar method.[21,24] Because the most intense fcc Ni peak (*111*) overlaps with the *011* peak of graphite, the relative ratio of this peak to other graphite peaks can be used to infer that Ni is present (Figure S6). TEM and EDS further confirm the presence of Ni nanoparticles supported on graphite. Figure 8b shows a TEM image with small, spherical particles supported on the graphite, with the *200* peak of fcc Ni indicated on the SAED pattern.

After reaction with TOP, the graphite-supported Ni nanoparticles convert to Ni_2P. The peak in the XRD pattern at 40.7° 2θ is consistent with the $\bar{2}11$ reflection of Ni_2P, and the breadth of the peak is as expected based on retaining the small particle size of the Ni precursor in the Ni_2P product (Figure 8a). Figure 8c shows a TEM micrograph of supported Ni_2P, which shows that the morphology and size are indeed conserved during the chemical transformation. SAED and EDS also confirm that Ni_2P is present: the $\bar{2}11$ peak is visible in the SAED pattern and the phosphorus content increases significantly as compared to the supported Ni particles, which only contain a small amount of phosphorus from the phosphine stabilizer (Figure 8c). Formation of supported Ni_2P nanocrystals by this method is significant because it provides an alternative to the higher temperature methods involving H_2 reduction of nickel phosphates[4,33] or use of phosphine gas as a phosphorus source in a reaction with supported nickel.[34]

Further versatility of this "conversion chemistry" approach for forming metal phosphides is demonstrated by the on-support conversion of microscale lithographically defined metal patterns into metal phosphide patterns. Copper stripes photolithographically patterned on a glass substrate (Figure 9a) can be converted to Cu_3P stripes (Figure 9b) by heating the Cu-patterned glass in TOP at 320 °C for 30 min. SEM micrographs (Figure 9) show that while the linear features of the Cu pattern and the center-to-center distance between stripes remain unchanged in the Cu_3P product, their width decreases and they begin to curl up at the edges, indicating that the adhesion between the glass and the copper is somewhat compromised during reaction with hot TOP. The EDS spectrum (Figure 9e) and element maps (Figure 9d,f) show that the stripes are composed of both copper and phosphorus. While the conversion reaction is harsh (in this case, resulting in diminished quality of the patterned features for the product), it represents an important proof-of-concept that on-substrate conversions are possible and implies that systems with better adhesion to a substrate can be converted into phosphides using this strategy. Work along these lines is in progress.

Conclusions

In this paper, we have shown that a surprisingly large number of metals can be converted into metal phosphides by reacting them in solution with TOP at moderate temperatures. This strategy appears to be general for many transition-metal and post-transition-metal systems. In addition, TOP can be used to convert not only metal nanocrystals into metal phosphides but also bulk-scale metal powders, foils, wires, films, supported nanocrystals, and patterned substrates. Considering the number of systems and diversity of morphologies and length scales over which the chemistry can occur, this represents a general, unified, and robust strategy for forming metal phosphides using readily available reagents and metal precursors. Furthermore, since there is some degree of morphology retention between the metal precursors and metal phosphide products, it may be possible to use this chemistry to more rigorously control the size, dispersity, and shape of a wide range of metal phosphide nanocrystals. Finally, since crystalline metal phosphides can be formed at low temperatures (<370 °C), this represents an alternative to traditional high-temperature and flux-based strategies for synthesizing metal phosphides and as such may lead to new nonequilibrium phases.

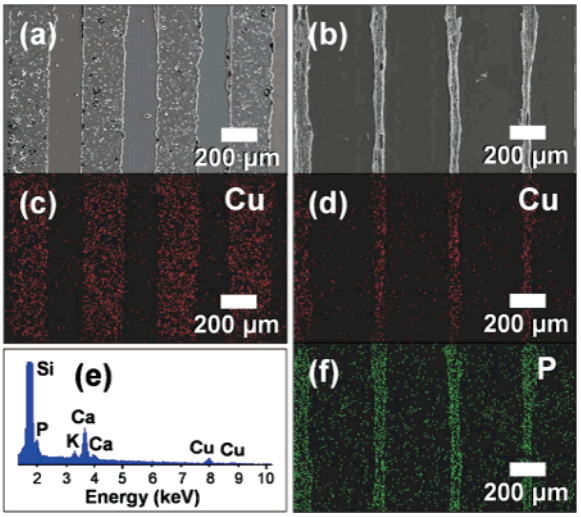

Figure 9. Microstructured Cu_3P patterns on a glass substrate made by reacting lithographically patterned glass-supported Cu patterns with hot TOP: (a) SEM image and (c) EDS map of lithographically patterned Cu stripes; (b) SEM image and (d,f) EDS map of Cu_3P stripes; (e) EDS spectrum for Cu_3P stripes (Ca, K, and Si are present in the glass substrate).

Acknowledgment. This work was supported by a NSF CAREER Award (DMR-0545201) and the Robert A. Welch Foundation (Grant No. A-1583). This material is based upon work supported under a NSF Graduate Fellowship to A.E.H. Partial support was also provided by the Arnold and Mabel Beckman Foundation (Young Investigator Award), DuPont (Young Professor Grant), and the Texas Advanced Research Program (Grant No. 010366-0002-2006). Electron microscopy was performed at the Texas A&M Microscopy and Imaging Center. Optical microscopy and photolithography were performed at the TAMU/CIMS Materials Characterization Facility. The authors thank Dr. Mike Pendleton at the Microscopy and Imaging Center for assistance with collecting SEM data and Jixin Chen for assistance with collecting UV−vis data.

Supporting Information Available: Histograms of nanocrystal sizes and additional XRD and EDS data. This material is available free of charge via the Internet at http://pubs.acs.org.

CM071021W

(33) Yang, S.; Liang, C.; Prins, R. *J. Catal.* **2006**, *241*, 465−469.
(34) Yang, S.; Prins, R. *Chem. Commun.* **2005**, 4178−1480.